Laser and Particle Beams (2017), *35*, 476–482.
© Cambridge University Press, 2017 0263-0346/17
doi:10.1017/S0263034617000490

Near-microcoulomb multi-MeV electrons generation in laser-driven self-formed plasma channel

Y. YANG,[1] J. JIAO,[1] C. TIAN,[1] Y. WU,[1,2] K. DONG,[1] W. ZHOU,[1,2] Y. GU,[1,2] AND Z. ZHAO[1,2]

[1]Science and Technology on Plasma Physics Laboratory, Laser Fusion Research Center, China Academy of Engineering Physics, P.O. Box 919-986, Mianyang 621900, People's Republic of China
[2]IFSA Collaborative Innovation Center, Shanghai Jiao Tong University, Shanghai 200240, People's Republic of China

(Received 8 April 2017; Accepted 18 May 2017)

Abstract

The origin and characteristics of near-microcoulomb multi-MeV electrons accelerated by short pulse lasers interacting with near-critical density plasma in self-formed channels are studied using three-dimensional particle-in-cell simulations. According to the analysis on interaction phenomena and electron dynamics, the dominant mechanism turns out to be direct laser acceleration, which ensures the outstanding energy coupling. Additionally, self-channeling is found to be a decisive factor for the acceleration performance, as electrons obtain ultra-high energy through betatron resonance inside the channels. In our findings, by using a relativistic short laser pulse and near-critical plasma, a large amount of energetic electrons can be generated, presenting a promising and accessible route to ultraintense, high-spatial-resolution radiation pulses.

Keywords: High-charge electron; Near-critical density; Plasma channel; Direct laser acceleration

1. INTRODUCTION

Ultrafast micro spot laser–plasma X-ray source has attracted much attention with excellence of short duration, small spot size, narrow divergence angle, controllable energy, etc. (Courtois *et al*., 2009; Compant La Fontaine *et al*., 2012) These advantages make this novel radiation source a promising diagnostic technique for multi applications (Westover *et al*., 2010), including shock waves, transient dynamics (Courtois *et al*., 2011), matter phase change and measurements on inner structures of high-atomic-number materials (Glinec *et al*., 2005; Brambrink *et al*., 2009; Courtois *et al*., 2013). To produce the bright high-spatial-resolution X-ray source, large numbers of tightly focused hot electrons with controllable energy are desired.

For years, scientists have been pursuing production of highly collimated, high-energy, high-charge electron beams (Adachi *et al*., 2006; Chen *et al*., 2007; Xu *et al*., 2010). Electron acceleration from LPIs (laser–plasma interactions), as a feasible and efficient method, has been studied in details (Wang *et al*., 2000; Pukhov & Meyer-ter-Vehn, 2002; Yu *et al*., 2003; Krygier *et al*., 2014). In 1999, Gahn *et al*. generated high-charge hot electrons in experiments via direct laser acceleration (DLA). They presented an optimal density of 0.2 n_c to accelerate 3.2 nC electrons to maximum effective temperature of 3.3 MeV, corresponding to an energy conversion efficiency of 5% (Gahn *et al*., 1999). Later in 2001, Santala *et al*. stressed the self-modulated laser wakefield acceleration (SMLWFA) in their experiments where the electron temperature exceeds 8 MeV, the charge reaches 64 nC (>10 MeV), and a conversion efficiency exceeds 2% (Santala *et al*., 2001). Similar conclusion is made by Malka *et al*., and they measured 8 nC electrons with maximum energy of 70 MeV from a 600 mJ laser pulse (Malka *et al*., 2001). Then in 2007, Chen *et al*. observed long plasma channel during the self-guiding of a 100 TW, 30 fs laser. The centimeter-scale channel formation made the hot electron charge (>1 MeV) to 10 nC per shot (Chen *et al*., 2007). Moreover, scientists proposed methods such as large focal spots (Xu *et al*., 2010) and multiple intensity peaks (Shen *et al*., 2012) to generate large or more bubbles in the wakefield regime, aiming at accelerating more electrons. For instance, Shen *et al*. just obtained 21 MeV electron bunches of 22 nC in multi-bubble wake structure produced by a multi-peaked pulse of 100 TW and 30 fs (Shen *et al*., 2012).

According to existing works, there are two major schemes for producing large-current relativistic electrons: DLA

Address correspondence and reprint requests to: Z. Zhao, Science and Technology on Plasma Physics Laboratory, Laser Fusion Research Center, China Academy of Engineering Physics, P.O. Box 919-986, Mianyang 621900, People's Republic of China. E-mail: zhaozongqing99@caep.cn

https://doi.org/10.1017/S0263034617000490 Published online by Cambridge University Press

(Gahn *et al*., 1999; Pukhov *et al*., 1999; Naseri *et al*., 2012; Toncian *et al*., 2016) and SMLWFA (Santala *et al*., 2001; Masuda *et al*., 2007; Shen *et al*., 2012). They will compete with each other or even co-exist in the same interaction (Malka *et al*., 2001; Pukhov & Meyer-ter-Vehn, 2002; Adachi *et al*., 2006; Kneip *et al*., 2008; Shaw *et al*., 2014), and their underlying physics can be understood as below. As the laser propagates, its ponderomotive force pushes plasma electrons both longitudinally and transversely to leave the pulse region, making a density destabilization. For the SMLWFA, the laser pulse will break up into pulselets and excite a series of plasma waves after the propagation. The enhanced wakefields thus exchange energy with lots of electrons in the axial direction (Ting *et al*., 1997; Mangles *et al*., 2005). In DLA, a positively charged plasma channel associated with charge-separated field is formed, which makes trapped electrons to do betatron oscillations (Shaw *et al*., 2014). The transverse momentum of electron then can be converted in longitudinal direction via $v \times B$ force. Among these two regimes, the electron cavitation and oscillation are essentially needed, while the only difference lies on the origin of the energy gain. Furthermore, for fixed laser parameters, they share relatively high plasma densities in common.

Therefore, near-critical density (NCD) plasma is put forward to obtain high-yield energetic electrons (Gu *et al*., 2011; Iwawaki *et al*., 2014; Wang *et al*., 2015; Toncian *et al*., 2016). This density region not only enables the efficient acceleration mechanisms to happen, but also takes advantage of both the superiorities of gas and dense plasmas, resulting in intense energy absorption along with stronger and faster processes (Gahn *et al*., 1999; Liu *et al*., 2015). Other effects such as generation of quasi-static field, self-focusing, and self-channeling may be able to react to the interaction, thus further improving the acceleration effect.

In this paper, we make detailed investigations on the laser-driven electron acceleration in NCD plasma via simulation, reporting a high-current electron beam produced by the DLA mechanism. It is proven that a 10 J short laser pulse interacting with NCD plasma can generate near-microcoulomb (μC) multi-MeV electrons with remarkable energy gain. The physical scheme of this interaction is clarified in terms of electron characteristics and acceleration mechanism. It appears that self-channeling plays a key role in the hot electron production. Finally, optimization solution on initial parameters is discussed depending on parameter studies to satisfy the requirement for high-quality bright X-ray source production.

2. PARTICLE-IN-CELL (PIC) SIMULATION

In our research, the conditions of laser and plasma are of great importance to generating high-yield electron beam. Therefore, an appropriate proposal on simulation parameter settings is necessary. To our knowledge, there are two prerequisites for the presence of SMLWFA and DLA. It is well known that DLA relies on relativistic self-focusing, so the laser power should exceed the critical value $P_c \approx 17.5(\omega/\omega_p)^2$ (GW), where ω and ω_p respectively represent the frequency of laser and plasma (Pukhov & Meyer-ter Vehn, 1996; Gibbon, 2005). For the SMLWFA, it differs from LWFA based on the premise that the pulse duration $\tau \gg \lambda_{pe}/c$, where $\lambda_{pe} = c/\omega_{pe}$ is the plasma wavelength (Shaw *et al*., 2014). Hence, initial parameters are properly chosen to meet the requirements, aiming at more electrons to be heated.

We have carried out three-dimensional simulations using a fully relativistic PIC code VORPAL (Nieter & Cary, 2004). The simulation box is $60\lambda(x) \times 20\lambda(y) \times 20\lambda(z)$ with $600 \times 200 \times 200$ grid cells and each cell contains eight macro-particles. A relativistic short laser pulse (with wavelength $\lambda = 1$ μm) linearly polarized in y direction is considered. The pulse is incident along the x-axis with a spatial Gaussian envelop $a = a_0 \exp[-(y^2 + z^2)/w_0^2]$, where $a_0 = eE_L/m_e\omega c = 10$ is the normalized laser vector potential, $w_0 = 6\lambda$ is the beam waist. Its temporal profile is expressed as $f(t) = \sin^2(\pi t/2\tau)$ $(0 \le t \le 2\tau)$, and $\tau = 60$ fs. The corresponding laser peak intensity is $I \approx 1.38 \times 10^{20}$ W/cm^2, so the peak power $P = \pi w_0^2 I \approx 156.07$ TW. Since we want the laser to achieve an optimal focusing state, the density of uniform CH plasma is set to be the optimal near-critical value (Shou *et al*., 2016) $n_e = 0.12 a_0 n_c = 1.2\ n_c$, where $n_c = m_e\omega^2/4\pi e^2$ is the critical plasma density. In this case, the plasma wavelength, $\lambda_{pe} \approx 0.14\ \mu m \ll c\tau$, and the peak laser power, $P \gg P_c \approx 14.6$ GW, which satisfy the aforementioned demands. The pulse duration also overlaps the trapped electrons for DLA (Shaw *et al*., 2014).

In our analysis, we count in all the electrons (with a kinetic energy $E_k > 0.5$ MeV and forward momentum) both inside and out of the simulation box after the incidence. Simulation results show that, when the laser is almost depleted in the plasma, the total electron charge is up to 645 nC. The effective temperature of the electrons reaches 6.83 MeV, and the cut-off energy exceeds 100 MeV, showing a considerable energy gain. The energy enhancement is well above the ponderomotive energy of the laser according to the scaling law (Wilks *et al*., 1992)

$$T = 0.511((1 + a_0^2/2)^{1/2} - 1)(\text{MeV}) = 3.138\,\text{MeV}.$$

At the moment of 160 fs, the laser is self-focused to a peak intensity, accompanied by a strong electron acceleration. As seen from Figure 1a, the amplitude of pulse reaches 35.73 with a spot radius of 0.92 μm. Meanwhile, background electrons are expelled outwards to generate a region devoid of plasma electrons. In Figure 1b, a circular quasi-static magnetic field is created around the light axis, with its strength up to 526 MG, strong enough to trap electrons to build the channel wall, thus confining the propagating pulse as well. Figure 1c, 1d show the electron density distributions on different planes, and only in (x, y) section can we see the zigzag trajectory of electron bunches with a period of about 1λ. They imply that electrons inside the channel oscillate along the

https://doi.org/10.1017/S0263034617000490 Published online by Cambridge University Press

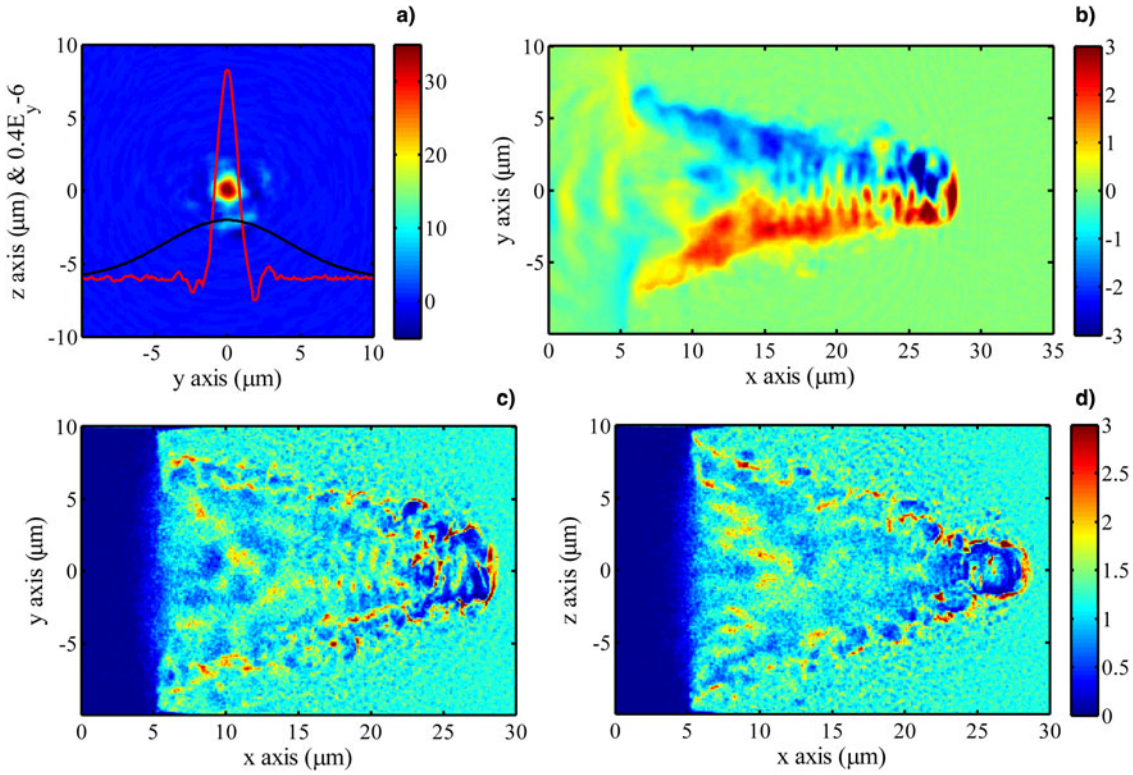


Fig. 1. Focusing state at $t = 160$ fs: (a) (y, z) section of E_y (in unit of $m_e c\omega/e$) at focal position and normalized E_y along the y-axis at $z = 0$ μm, where black lines mark the initial laser transverse profile; (b, c) (x, y) section of (b) quasi-static magnetic field B_z (in unit of $m_e\omega/e$) and (c) electron density (in unit of n_c) at $z = 0$ μm; (d) (x, z) section of electron density (in unit of n_c) at $y = 0$ μm.

polarization direction of laser, ending up with a large forward current.

To fully understand the phenomena above, we explore the electron dynamics and acceleration mechanism. Here we identify the origin of electron energy gain by splitting them into components Γ_x and $\Gamma_\perp$, which are from longitudinal and transverse electric fields, respectively (Gahn *et al.*, 1999). The variables are expressed as

$$\Gamma_x = -\int_0^t \frac{2eE_z p_z}{(mc)^2} dt, \quad \Gamma_\perp = -\int_0^t \frac{2e\vec{E}_\perp \cdot \vec{p}_\perp}{(mc)^2} dt.$$

Attention should be paid that we only keep track of the energy gain within 20 fs at certain moment. Electron distributions with respect to gain components at different moments are measured. Typically as Figure 2a shows, most of the electrons gain energy from the transverse electric field, and only a minority of them are driven to quite low kinetics by longitudinal field. That apparently indicates the dominant role of DLA throughout the acceleration process, and longitudinal plasma waves play a minor role in this case. Also, energy spectrum of different electron groups, and high-energy electron distribution at $t = 200$ fs are respectively

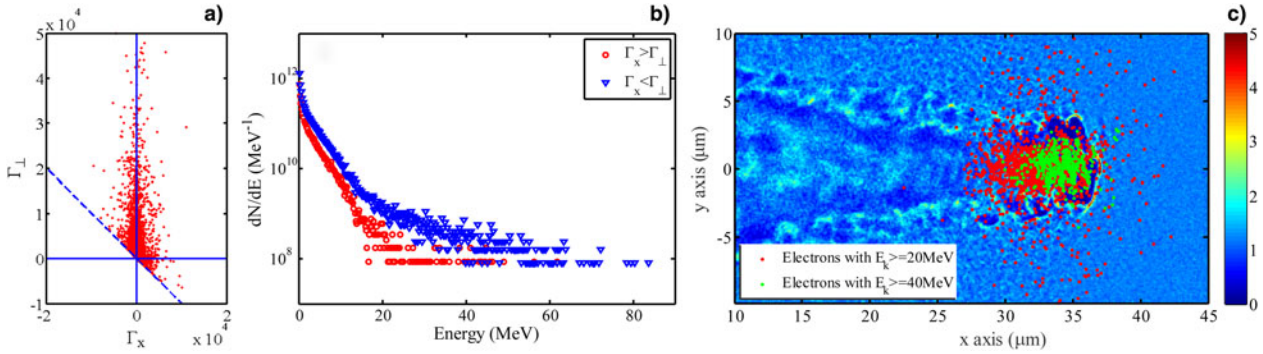


Fig. 2. Electron characteristics at $t = 200$ fs: (a) distribution of the accelerated electrons in the (Γ_x, $\Gamma_\perp$) space; (b) breakdown of electron spectrum with respect to the major acceleration mechanism; (c) electron density (in unit of n_c) and distribution at $z = 0$ μm.

https://doi.org/10.1017/S0263034617000490 Published online by Cambridge University Press

displayed in Figure 2b, 2c. We observe that most highly energetic electrons gain energy from transverse laser field undergoing transverse betatron motion in the channel, where the resonance happens when the oscillation frequency in polarization direction coincides with the laser frequency (Pukhov *et al*., 1999). The component of low-energy electrons mainly comes from the direct energy conversion via ponderomotive force, the same as those accelerated by longitudinal fields. The latter (marked by red circles) has an effective temperature of 3.17 MeV, consistent with the ponderomotive scaling law (3.138 MeV).

3. DISCUSSION

Based on the simulation results, the detailed scheme during this interaction can be clearly explained, which includes two effects: the laser self-focusing and the electron heating. Firstly, the incident beam enters the plasma and becomes self-focused, forming a charge-separated field and a positively charged channel via the ponderomotive expulsion. The electrons outside the channel will gather at the pulse edge to build an overdense channel wall, whose density exceeds 7 n_c in simulations, in turn preventing the laser from scattering out. Meanwhile inside electrons make betatron motion under a combination of ponderomotive force, transverse electric field and self-magnetic pinching force (Mangles *et al*., 2005; Kneip *et al*., 2008). The ones resonant with the laser frequency in its polarization direction can gain considerable energy directly through $v \times B$ force. As a result, the production of high-energy electron strongly depends on the betatron resonance, whose precondition is the self-tightly-formed channel with sharp boundaries.

Now we investigate three crucial parameters that characterize the acceleration performance during the interaction: the peak amplitude of laser a_{max}, the total electron charge Q_e, and their effective temperature T_{eff}. Figure 3a displays the temporal evolution of these parameters. It shows that the electron temperature comes to a climax of 12.62 MeV at 200 fs. Electron spectrums at different moments are plotted in Figure 3b. At 200 fs, electrons with quite high energies grow significantly compared with initial condition, explaining the rise of the effective temperature. Later, some electrons turn back to low-energy state, and hence reduce their overall temperature. The degression of the electron temperature in later stage can be interpreted as below. After the laser energy has considerably deposited, the acceleration is gradually weakened. At the same time, fast electrons that reach the laser front or overtake the electrostatic potential building up at the plasma boundary, are likely to suffer an energy loss caused by the space charge field when escaping from the channel. Hence, high-energy electrons are partly reduced, resulting in the temperature drop (Pukhov *et al*., 1999).

To study the influence of initial parameters on the fast electron production, more simulations are carried out. Firstly, the plasma density is varied with unchanged laser parameters, and the results are showed in Table 1 and Figure 4a, 4b. As the density increases, the progress of interaction and energy deposition happens faster as expected, and channel length reduces with more instability and diffusion. Since the channel determines the effective acceleration distance of DLA, more electrons are able to achieve high energies in low-density plasma. Thereupon, their larger effective temperature is inversely correlated to the plasma density in Figure 4a. In addition, Figure 4b presents that total charge firstly grows as density decreases, then gets lower after $n_e < 0.4\ n_c$. At this point, the overlong propagation causes considerable energy loss, leading to the charge diminution. From the results one can easily conclude that, critical plasma (0.1–1 n_c) is able to produce near 0.6 μC electrons with temperature about 10 MeV by intense short lasers.

The dependence of electron characteristics on laser intensities is also discussed and displayed in Figure 4c, 4d. It is found that both the electron temperature and total charge are proportional to the intensity square root, implying the

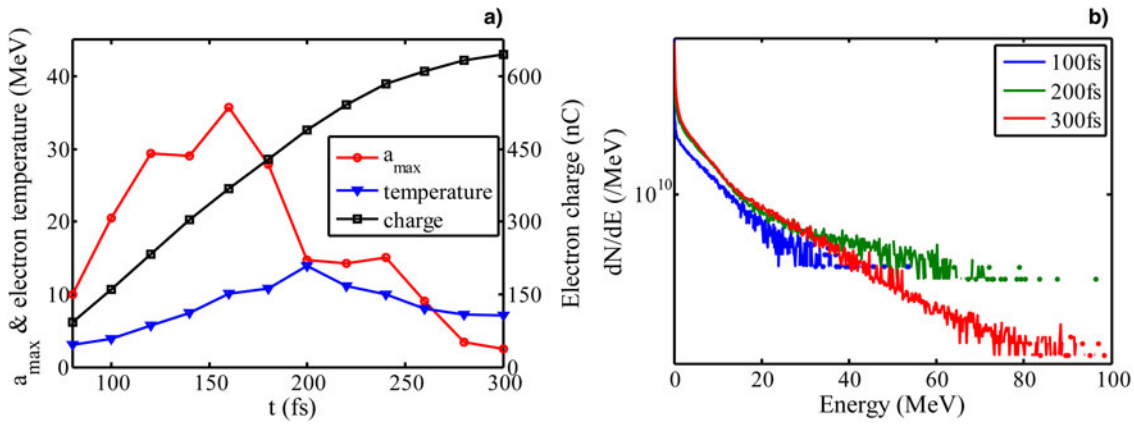


Fig. 3. (a) Temporal evolution: the peak amplitude of laser a_{max}, the total electron charge Q_e (in unit of nC), and the effective temperature of electron T_{eff} (in unit of MeV); (b) electron spectrums at different moments.

https://doi.org/10.1017/S0263034617000490 Published online by Cambridge University Press

Table 1. *Simulation results: values of diagnostic variables for different cases*

Plasma electron density (n_c)	0.1	0.2	0.4	0.8	1.2	2	3	4
Total charge of interested electrons (nC)	556	671	708	670	645	611	532	446
Larger effective temperature (MeV)	34.03	15.93	14.04	7.32	6.83	3.07	2.63	2.53
Channel length (μm)	295	175	111	62	49	36	24	14

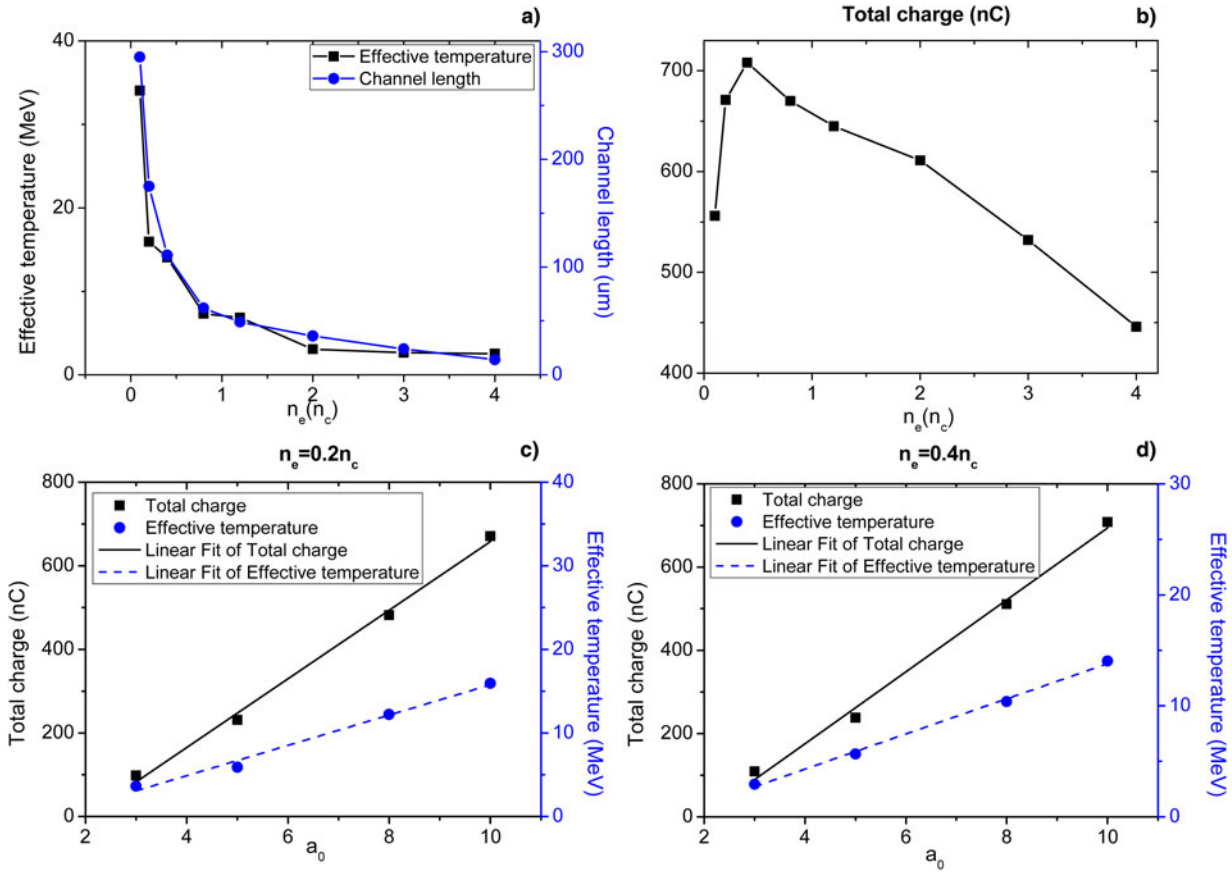


Fig. 4. (a) Channel length (in unit of μm) and $T_{\rm eff}$ (in unit of MeV) versus $n_{\rm e}$ (in unit of n_c); (b) $Q_{\rm e}$ (in unit of nC) versus $n_{\rm e}$; (c)(d) $Q_{\rm e}$ and $T_{\rm eff}$ versus a_0, the best fit gives scaling with (c) $\alpha \approx 1.54$ MeV, $\beta \approx 69.9$ nC ($n_{\rm e} = 0.2\ n_c$); (d) $\alpha \approx 1.35$ MeV, $\beta \approx 73.6$ nC ($n_{\rm e} = 0.4\ n_c$).

close relation between the laser energy and hot electron generation. Here we can give the scaling laws expressed as

$$T_{\rm eff} \sim \alpha\left(I/10^{18}\ {\rm W/cm^3}\right)^{1/2}, \quad Q_{\rm e} \sim \beta\left(I/10^{18}\ {\rm W/cm^3}\right)^{1/2}.$$

The coefficient are $\alpha \approx 1.54$ MeV, $\beta \approx 69.9$ nC for $n_{\rm e} = 0.2\ n_c$ and $\alpha \approx 1.35$ MeV, $\beta \approx 73.6$ nC for $n_{\rm e} = 0.4\ n_c$, in good accordance with the DLA scaling law with $\alpha \approx 1.5$ MeV (Pukhov *et al.*, 1999).

To sum up the discussion, the generation of high-charge, high-energy electrons hinges on three key factors: intense laser pulse, NCD plasma, and DLA mechanism. The required laser provides ponderomotive force sufficient to enable rapid self-channeling and strong acceleration. NCD plasma not only makes the energy deposits fast with little loss, but contributes to better laser focusing and channeling (Wang *et al.*, 2011; Shou *et al.*, 2016), offering a good environment for the DLA to take place. The laser focused to high contrast, high intensity, and micro spot is helpful to enhance the later energy absorption; and self-formed channel guides the pulse over Rayleigh length, allowing electrons to be accelerated continuously. In DLA, electrons directly get energy from laser field where they can be driven forward via transverse movement even under incomplete resonance, resulting in hot temperature, large yield as well as strong energy coupling.

https://doi.org/10.1017/S0263034617000490 Published online by Cambridge University Press

4. SUMMARY

In summary, the origin and characteristics of large-current energetic electrons generated by intense short laser pulses in NCD plasmas are studied. The electron beams heated by a 10 J laser reach a total charge near 0.7 μC with an effective temperature up to 10 MeV, indicating great energy conversion in laser–NCD plasma interactions. It is found that DLA predominate the acceleration, and the ultra-high-energy gain of electrons is observed to come from betatron resonance in self-formed channels. Three crucial conditions are demonstrated for the high-charge hot electron beam: high-intensity laser, NCD plasma, and self-channeling. Additionally, dependence of electron characteristics on different parameters is investigated in NCD range. For a given laser, low-density plasma provides higher electron temperature and longer channel. However, overlong propagation distance leads to inevitable energy dissipation and loss of electron yield. Therefore, we need to appropriately choose the target density with an overall consideration of electron energy, interaction efficiency and total charge in practice.

This work proves the robustness of NCD plasma to produce large amounts of multi-MeV electrons through DLA mechanism. It offers a promising and feasible access to the generation of brilliant bremsstrahlung source with micro spot and high spatial resolution, which is hopeful to realize monopulse transient imaging and potentially play significant roles in applications such as hydrodynamics, fast moving object monitoring, high-density sample compression visualization, and ICF implosion target imaging.

ACKNOWLEDGMENTS

This work is supported by the National Natural Science Foundation of China (NSFC) (grant numbers 11375161, 11405159, and 11505166), the Science and Technology on Plasma Physics Laboratory at CAEP (grant number 6142A04020102), the National key program for S&T Research and Development (grant number 2016YFA0401100), and the Science Challenge Program (Project No. JCKY2016212A505).

REFERENCE

Adachi, M., Miura, E., Kato, S., Koyama, K., Masuda, S., Watanabe, T., Okamoto, H., Ogata, A. & Tanimoto, M. (2006). Cascade acceleration of electrons by laser wakefield and direct laser field. *Jpn. J. Appl. Phys*. **45**, 4214–4218.

Brambrink, E., Wei, H.G., Barbrel, B., Audebert, P., Benuzzi-Mounaix, A., Boehly, T., Endo, T., Gregory, C., Kimura, T., Kodama, R., Ozaki, N., Park, H.-S., Rabec le Gloahec, M. & Koenig, M. (2009). X-ray source studies for radiography of dense matter. *Phys. Plasmas* **16**, 033101 (7 pp).

Chen, L.M., Kotaki, H., Nakajima, K., Koga, J., Bulanov, S.V., Tajima, T., Gu, Y.Q., Peng, H.S., Wang, X.X., Wen, T.S., Liu, H.J., Jiao, C.Y., Zhang, C.G., Huang, X.J., Guo, Y., Zhou, K.N., Hua, J.F., An, W.M., Tang, C.X. & Lin, Y.Z. (2007). Self-guiding of 100 TW femtosecond laser pulses in centimeter-scale underdense plasma. *Phys. Plasmas* **14**, 040703 (4 pp).

Compant La Fontaine, A., Courtois, C. & Lefebvre, E. (2012). Production of multi-MeV Bremsstrahlung x-ray sources by petawatt laser pulses on various targets. *Phys. Plasmas* **19**, 023104 (10 pp).

Courtois, C., Compant La Fontaine, A., Landoas, O., Lidove, G., Méot, V., Morel, P., Nuter, R., Lefebvre, E., Boscheron, A., Grenier, J., Aléonard, M.M., Gerbaux, M., Gobet, F., Hannachi, F., Malka, G., Scheurer, J.N. & Tarisien, M. (2009). Effect of plasma density scale length on the properties of bremsstrahlung x-ray sources created by picosecond laser pulses. *Phys. Plasmas* **16**, 013105 (12 pp).

Courtois, C., Edwards, R., Compant La Fontaine, A., Aedy, C., Barbotin, M., Bazzoli, S., Biddle, L., Brebion, D., Bourgade, J.L., Drew, D., Fox, M., Gardner, M., Gazave, J., Lagrange, J.M., Landoas, O., Le Dain, L., Lefebvre, E., Mastrosimone, D., Pichoff, N., Pien, G., Ramsay, M., Simons, A., Sircombe, N., Stoeckl, C. & Thorp, K. (2011). High-resolution multi-MeV x-ray radiography using relativistic laser-solid interaction. *Phys. Plasmas* **18**, 023101 (5 pp).

Courtois, C., Edwards, R., Compant La Fontaine, A., Aedy, C., Bazzoli, S., Bourgade, J.L., Gazave, J., Lagrange, J.M., Landoas, O., Le Dain, L., Mastrosimone, D., Pichoff, N., Pien, G. & Stoeckl, C. (2013). Characterisation of a MeV Bremsstrahlung x-ray source produced from a high intensity laser for high areal density object radiography. *Phys. Plasmas* **20**, 083114 (9 pp).

Gahn, C., Tsakiris, G.D., Pukhov, A., Meyer-ter-Vehn, J., Pretzler, G., Thirolf, P., Habs, D. & Witte, K.J. (1999). Multi-MeV electron beam generation by direct laser acceleration in high-density plasma channels. *Phys. Rev. Lett*. **83**, 4772–4775.

Gibbon, P. (2005). Short pulse laser interactions with matter. In *Propagation of Finite-Width Laser Pulses* (Garden, C., Ed.), pp. 96–97. London: Imperial College Press.

Glinec, Y., Faure, J., Le Dain, L., Darbon, S., Hosokai, T., Santos, J.J., Lefebvre, E., Rousseau, J.P., Burgy, F., Mercier, B. & Malka, V. (2005). High-resolution γ-ray radiography produced by a laser–plasma driven electron source. *Phys. Rev. Lett*. **94**, 025003 (4 pp).

Gu, Y.J., Kong, Q., Li, Y.Y., Ban, H.Y., Zhu, Z. & Kawata, S. (2011). Steady plasma channel formation and particle acceleration in an interaction of an ultraintense laser with near-critical density plasma. *Phys. Plasmas* **18**, 030704 (4 pp).

Iwawaki, T., Habara, H., Baton, S., Morita, K., Fuchs, J., Chen, S., Nakatsutsumi, M., Rousseaux, C., Filippi, F., Nazarov, W. & Tanaka, K.A. (2014). Collimated fast electron beam generation in critical density plasma. *Phys. Plasmas* **21**, 113103 (8 pp).

Kneip, S., Nagel, S.R., Bellei, C., Bourgeois, N., Dangor, A.E., Gopal, A., Heathcote, R., Mangles, S.P.D., Marquès, J.R., Maksimchuk, A., Nilson, P.M., Ta Phuoc, K., Reed, S., Tzoufras, M., Tsung, F.S., Willingale, L., Mori, W.B., Rousse, A., Krushelnick, K. & Najmudin, Z. (2008). Observation of synchrotron radiation from electrons accelerated in a petawatt-laser-generated plasma cavity. *Phys. Rev. Lett*. **100**, 105006 (4 pp).

Krygier, A.G., Schumacher, D.W. & Freeman, R.R. (2014). on the origin of super-hot electrons from intense laser interactions with solid targets having moderate scale length preformed plasmas. *Phys. Plasmas* **22**, 023112 (8 pp).

Liu, B., Hu, R.H., Wang, H.Y., Wu, D., Liu, J., Chen, C.E., Meyer-ter-Vehn, J., Yan, X.Q. & He, X.T. (2015). Quasimonoenergetic electron beam and brilliant gamma-ray radiation generated from near critical density plasma due to relativistic resonant phase locking. *Phys. Plasmas* **22**, 080704 (5 pp).

https://doi.org/10.1017/S0263034617000490 Published online by Cambridge University Press

Malka, V., Faure, J., Marquès, J.R., Amiranoff, F., Rousseau, J.P., Ranc, S., Chambaret, J.P., Najmudin, Z., Walton, B., Mora, P. & Solodov, A. (2001). Characterization of electron beams produced by ultrashort (30fs) laser pulses. *Phys. Plasmas* **8**, 2605–2608.

Mangles, S.P.D., Walton, B.R., Tzoufras, M., Najmudin, Z., Clarke, R.J., Dangor, A.E., Evans, R.G., Fritzler, S., Gopal, A., Hernandez-Gomez, C., Mori, W.B., Rozmus, W., Tatarakis, M., Thomas, A.G.R., Tsung, F.S., Wei, M.S. & Krushelnick, K. (2005). Electron acceleration in cavitated channels formed by a petawatt laser in low-density plasma. *Phys. Rev. Lett*. **94**, 245001 (4 pp).

Masuda, S., Miura, E., Koyama, K., Kato, S., Adachi, M., Watanabe, T., Torii, K. & Tanimoto, M. (2007). Energy scaling of monoenergetic electron beams generated by the laser-driven plasma based accelerator. *Phys. Plasmas* **14**, 023103 (8 pp).

Naseri, N., Pesme, D., Rozmus, W. & Popov, K. (2012). Channeling of relativistic laser pulses, surface waves, and electron acceleration. *Phys. Rev. Lett*. **108**, 105001 (4 pp).

Nieter, C. & Cary, J.R. (2004). VORPAL: A versatile plasma simulation code. *J. Comput. Phys*. **196**, 448–473.

Pukhov, A. & Meyer-ter Vehn, J. (1996). Relativistic magnetic self-channeling of light in near-critical plasma: Three dimensional particle-in-cell simulation. *Phys. Rev. Lett*. **76**, 3975–3978.

Pukhov, A. & Meyer-ter-Vehn, J. (2002). Laser wake field acceleration: The highly non-linear broken-wave regime. *Appl. Phys. B* **74**, 355–361.

Pukhov, A., Sheng, Z.-M. & Meyer-ter-Vehn, J. (1999). Particle acceleration in relativistic laser channels. *Phys. Plasmas* **6**, 2847–2854.

Santala, M.I.K., Najmudin, Z., Clark, E.L., Tatarakis, M., Krushelnick, K., Dangor, A.E., Malka, V., Faure, J., Allott, R. & Clarke, R.J. (2001). Observation of a hot high-current electron beam from a self-modulated laser wakefield accelerator. *Phys. Rev. Lett*. **86**, 1227–1230.

Shaw, J.L., Tsung, F.S., Vafaei-Najafabadi, N., Marsh, K.A., Lemos, N., Mori, W.B. & Joshi, C. (2014). Role of direct laser acceleration in energy gained by electrons in a laser wakefield accelerator with ionization injection. *Plasma Phys. Control. Fusion* **56**, 084006 (7 pp).

Shen, B., Wu, Y., Dong, K., Zhu, B., Gu, Y., Ji, L., Jiao, C., Teng, J., Hong, W., Zhao, Z., Cao, L., Wang, X. & Yu, M. (2012). High-charge energetic electron bunch generated by 100 TW laser pulse. *Phys. Plasmas* **19**, 033106 (5 pp).

Shou, Y.R., Lu, H.Y., Hu, R.H., Lin, C., Wang, H.Y., Zhou, M.L., He, X.T., Chen, J.E. & Yan, X.Q. (2016). Near-diffraction-limited laser focusing with a near-critical density plasma lens. *Opt. Lett*. **41**, 139–142.

Ting, A., Moore, C.I., Krushelnick, K., Manka, C., Esarey, E., Sprangle, P., Hubbard, R., Burris, H.R., Fischer, R. & Baine, M. (1997). Plasma wakefield generation and electron acceleration in a self-modulated laser wakefield accelerator experiment. *Phys. Plasmas* **4**, 1889–1899.

Toncian, T., Wang, C., McCary, E., Meadows, A., Arefiev, A.V., Blakeney, J., Serratto, K., Kuk, D., Chester, C., Roycroft, R., Gao, L., Fu, H., Yan, X.Q., Schreiber, J., Pomerantz, I., Bernstein, A., Quevedo, H., Dyer, G., Ditmire, T. & Hegelich, B.M. (2016). Non-Maxwellian electron distributions resulting from direct laser acceleration in near-critical plasmas. *Matter Radiat. Extrem*. **1**, 82–87.

Wang, H.Y., Lin, C., Sheng, Z.M., Liu, B., Zhao, S., Guo, Z.Y., Lu, Y.R., He, X.T., Chen, J.E. & Yan, X.Q. (2011). Laser shaping of a relativistic intense, short Gaussian pulse by a plasma lens. *Phys. Rev. Lett*. **107**, 265002 (5 pp).

Wang, J., Zhao, Z.Q., Zhu, B., Zhang, Z.M., Cao, L.H., Zhou, W.M. & Gu, Y.Q. (2015). Refluxed electrons direct laser acceleration in ultrahigh laser and relativistic critical density plasma interaction. *Phys. Plasmas* **22**, 013106 (6 pp).

Wang, X., Krishnan, M., Saleh, N., Wang, H. & Umstadter, D. (2000). electron acceleration and the propagation of ultrashort high-intensity laser pulses in plasmas. *Phys. Rev. Lett*. **84**, 5324–5327.

Westover, B., MacPhee, A., Chen, C., Hey, D., Ma, T., Maddox, B., Park, H.-S., Remington, B. & Beg, F.N. (2010). Study of silver Kα and bremsstrahlung radiation from short-pulse laser-matter interactions with applications for x-ray radiography. *Phys. Plasmas* **17**, 082703 (5 pp).

Wilks, S.C., Kruer, W.L., Tabak, M. & Langdon, A.B. (1992). Absorption of ultra-intense laser pulses. *Phys. Rev. Lett*. **69**, 1383–1386.

Xu, J., Shen, B., Zhang, X., Wen, M., Ji, L., Wang, W., Yu, Y. & Nakajima, K. (2010). Generation of a large amount of energetic electrons in complex-structure bubble. *New J. Phys*. **12**, 023037 (9 pp).

Yu, M.Y., Yu, W., Chen, Z.Y., Zhang, J., Yin, Y., Cao, L.H., Lu, P.X. & Xu, Z.Z. (2003). Electron acceleration by an intense short-pulse laser in underdense plasma. *Phys. Plasmas* **10**, 2468–2474.

https://doi.org/10.1017/S0263034617000490 Published online by Cambridge University Press